Available online at www.sciencedirect.com
SCIENCE DIRECT®
International Journal of Plasticity 21 (2005) 1009–1039
INTERNATIONAL JOURNAL OF Plasticity
www.elsevier.com/locate/ijplas

Linear transfomation-based anisotropic yield functions

F. Barlat [a,d,*], H. Aretz [b], J.W. Yoon [a,d], M.E. Karabin [a], J.C. Brem [a], R.E. Dick [c]

[a] *Materials Science Division, Alcoa Technical Center, 100 Technical Drive, Alcoa Center, PA 15069-0001, USA*
[b] *LASSO Ingenieurgesellschaft mbH, Markomannenstrasse 11, 70771 Leinfelden-Echterdingen, Germany*
[c] *Rigid Packaging Division Technology, Alcoa Technical Center, 100 Technical Drive, Alcoa Center, PA 15069-0001, USA*
[d] *Center for Mechanical Technology and Automation, University of Aveiro, Aveiro 3810, Portugal*

Received in final revised form 7 June 2004
Available online 12 September 2004

Abstract

In this paper, anisotropic yield functions based on linear transformations of the stress deviator are discussed in general terms. Two specific convex formulations are proposed to describe the anisotropic behavior of metals and alloys for a full stress state (3D). The type of input data recommended for the description of plastic anisotropy in sheet samples is discussed. The two formulations are shown to be suitable constitutive models for 6111-T4 and 2090-T3 aluminum alloy sheet samples.

Keywords: Anisotropic material; Constitutive behaviour; Metallic material; Polycrystalline material; Mechanical testing

* Corresponding author. Tel.: +1 724 337 3920; fax: +1 724 337 2044.
E-mail address: frederic.barlat@alcoa.com (F. Barlat).

0749-6419/$ - see front matter © 2004 Elsevier Ltd. All rights reserved.
doi:10.1016/j.ijplas.2004.06.004

1. Introduction

Plastic anisotropy in metals and alloys is the result of different features of the material microstructure. At moderate temperature, plastic deformation occurs mainly by glide of dislocations and possibly, depending on the material, by twinning. These mechanisms operate on given crystallographic planes and in certain directions. As a result, the most critical feature leading to anisotropy is crystallographic texture, i.e., the distribution of grain orientations. However, other features, such as the grain shape, contribute as well because they influence how different grains are interacting with each other, thus promoting the slip activity on certain crystallographic slip planes and directions.

The polycrystal description of plastic anisotropy has been very successful over the last few decades. This approach is based on the physical aspects of plastic deformation, slip and twinning in crystals, and on averaging procedures over a large number of grains. The crystallographic texture is the main input to these models but other parameters, such as the grain shape, can also be included. Because polycrystal models can track the lattice rotation of each individual grain, the material anisotropy naturally evolves, which makes this approach very attractive. However, as a drawback, these models are computationally time-intensive when they are used in the simulations of metal forming processes.

At the continuum scale, for a multiaxial stress space, plastic deformation is well described with a yield surface, a flow rule and a hardening law. Plastic anisotropy is the result of the distortion of the yield surface shape due to the material microstructural state. Życzkowski (1981) discussed different phenomena attached to the yield surface shape at a macroscopic scale. Regardless of the shape of the yield surface, strain hardening can be isotropic or anisotropic. The former corresponds to an expansion of the yield surface without distortion. Any other form of hardening is anisotropic and leads to different properties in different directions after deformation, even if the material is initially isotropic. For instance, Barlat and Liu (1998) used a kinematic hardening model, defined by the translation of the yield surface, to explain the influence of precipitates on plastic anisotropy in artificially aged binary Al–Cu alloys.

The present paper is not concerned about the evolution of the yield surface but about its shape. Whether the yield surface expands, translates or rotates as plastic deformation proceeds, a shape must be defined to account for initial anisotropy. If the yield surface distorts during deformation, a unique shape can be used to describe an average material response over a certain deformation range. Because mechanical data are used as input, these models can be more accurate than polycrystal models when the strain is moderate. This is typically the case for sheet forming. However, for larger strains and for abrupt strain path changes, evolution is an issue and is the subject of much research at the present time (for instance, see Teodosiu and Hu, 1998; Peeters et al., 2001). Nevertheless, the descriptions of plastic anisotropy based on the concept of yield surfaces are convenient and time-efficient for engineering applications such as forming process simulations.

Certain properties of the continuum yield functions can be obtained from microstructural considerations. Bishop and Hill (1951) showed that for a single crystal obeying the Schmid law, i.e., dislocation glide occurs when the resolved shear stress on a slip system reaches a critical value, the resulting yield surface was convex and the associated strain increment was normal to it. Furthermore, they extended this result for a polycrystal by averaging the behavior of a representative number of grains in an elementary volume without making any assumption about the interaction mode between grains or the uniformity of the deformation gradient. Hecker (1976) reviewed many multiaxial experiments and did not find any clear contradiction to these assumptions on normality and convexity. Therefore, these properties are assumed to hold as a good approximation in the rest of this paper. From the normality flow rule, also known as the associated flow rule, the yield function ϕ serves as a plastic potential. For an isotropic material, the plastic strain increments $\mathrm{d}\varepsilon_i$ are proportional to the gradient of ϕ with respect to the principal stresses σ_1, σ_2 and σ_3

$$\mathrm{d}\varepsilon_i = \mathrm{d}\lambda \frac{\partial \phi}{\partial \sigma_i}. \tag{1}$$

In the above equation, $\mathrm{d}\lambda$ adjusts for the size of the strain increment. It is worth noting that Spitzig et al. (1976, 1984) conducted experiments under hydrostatic confinement and found a linear dependence between the mean stress (σ_m) and a measure of the effective stress (the second invariant of the stress deviator J_2). The volume changes that they observed experimentally were negligible compared to those calculated by assuming the classical associated flow rule. They concluded that plastic flow was non-associated, i.e., the strain increment was not normal to the yield surface. Practically, because this departure from normality is very small, it can be neglected for low to medium strength materials and low confinement pressure.

The convexity of the yield surface leads to a unique relationship between the stresses and the strain increments, a useful property for numerical simulations involving plastic deformation. A function $\phi(\sigma_k)$ is convex with respect to its arguments σ_k if its Hessian matrix $\mathbf{H}$, i.e.,

$$H_{ij} = \frac{\partial^2 \phi}{\partial \sigma_i \, \partial \sigma_j} \tag{2}$$

is positive semi-definite (Rockafellar, 1972). Lippman (1970) showed that convexity is preserved from the principal reference frame to any other reference frame.

In developing a yield function, it is important that the formulation reduces to isotropy when the material is isotropic. Otherwise, spurious anisotropy effects can be produced. This can be achieved effectively by using criteria that are written in terms of invariants and to perform mathematical transformations on these invariants. Several sets of invariants have been used to describe isotropic properties, for instance, the principal stresses σ_1, σ_2 and σ_3 or the basic invariants of the stress tensor, I_1, I_2 and I_3 (Życzkowski, 1981). For classical plasticity where the influence of hydrostatic pressure is neglected, the principal deviatoric stresses s_1, s_2 and s_3 (with

$s_3 = -s_1 - s_2$) or the basic invariants of the stress deviator, $J_2 = I_2 - I_1^2/3$ and J_3 ($J_1 = 0$), can be used advantageously.

Many anisotropic yield functions have been proposed over the years, starting with the works of von Mises (1928) and Hill (1948). Representative phenomenological plastic potentials are reviewed more or less extensively in a number of publications, for instance, in Życzkowski (1981, 2001), Banabic (2001), Yu (2002) and Barlat et al. (2004). In this paper, the anisotropic yield functions are characterized by their formulation type (linear transformation-based or not), the stress state considered (plane stress, full stress), and the number of anisotropy coefficients. A plane stress state is very often sufficient for sheet forming applications while a full stress state is necessary for problems in which the three-dimensional nature cannot be simplified. A large number of anisotropy coefficients enable more details of the material anisotropy to be captured but at the expense of simplicity.

For the description of incompressible plastic anisotropy, Cazacu and Barlat (2001, 2003) introduced general transformations based on the theory of tensor representations (Wang, 1970; Liu, 1982). These general transformations operate on the 2nd and the 3rd invariants of the stress tensor and are compatible with the symmetry group of the material considered. This theory was applied recently to materials, such as HCP metals, exhibiting tension–compression yield asymmetry (Cazacu and Barlat, 2004). However, with this approach, the conditions for ensuring convexity of the yield surface are difficult to verify. For this reason, a particular case of this general theory, which is based on linearly transformed stress components, has received more attention. Linear transformations on the stress tensor were first introduced by Sobodka (1969) and Boehler and Sawczuck (1970). For plane stress and orthotropic material symmetry, Barlat and Lian (1989) combined the principal values of these transformed stress tensors with an isotropic yield function. Barlat et al. (1991) applied this method to a full stress state and Karafillis and Boyce (1993) generalized it as the so-called isotropic plasticity equivalent (IPE) theory with a more general yield function and a linear transformation that can accommodate other material symmetries.

Because the above functions were not able to capture the anisotropic behavior of aluminum sheet to a desirable degree of accuracy, Barlat et al. (2003) introduced two linear transformations operating on the sum of two yield functions in the case of plane stress (see also Banabic et al., 2004). Bron and Besson (2004) further extended Karafillis and Boyce's approach to two linear transformations. These recently proposed yield functions include more anisotropy coefficients and, therefore, give a better description of the anisotropic properties of a material. This is particularly obvious for the description of uniaxial tension properties. Note that, for this purpose, other approaches are possible. Tong (2004) proposed a plane stress formulation with the so-called intrinsic variables and Fourier series to increase the number of material coefficients. However, with the exception of the yield function proposed by Bron and Besson (2004), most of them were developed for plane stress states or do not fulfill the requirements for convexity. In the present paper two other 3D approaches, also based on linear transformations, are introduced.

In the next section, general aspects of linear transformations operating on the Cauchy stress tensor are reviewed. Section 3 discusses the input data needed for the calculation of anisotropic yield function coefficients. Section 4 introduces a 3D yield function that includes 18 anisotropy coefficients and illustrative examples are given. Section 5 introduces a second yield function with 13 parameters only.

2. Yield functions and linear transformations

In this paper, **x**, **y** and **z** denote three orthogonal material directions. Usually, these directions correspond to the symmetry axes resulting from the material processing history, but this is not a necessary condition as long as they refer to axes associated to the material. Any pressure independent isotropic yield function can take the general form

$$\phi = \phi(\mathbf{S}) = h(\bar{\varepsilon}), \tag{3}$$

where h is a function of a measure of the accumulated plastic strain $\bar{\varepsilon}$ (hardening function). **S** represents the principal values of the stress deviator, **s**. Interestingly, a yield condition proposed by Richmond and Spitzig (1980) that describes the pressure effect discussed above could essentially be rewritten in a form similar to Eq. (3), i.e.,

$$\phi = \phi(\mathbf{S}) = h(\bar{\varepsilon})\{1 - \alpha I_1\}, \tag{4}$$

where ϕ is, in this case, a homogenous function of degree 1, and α is the pressure coefficient. These authors found that the normality rule was holding as a good approximation of the flow rule in the deviatoric stress space and that the volume change was negligible. For steel and commercial purity aluminum, the measured values of α were found to be very small, i.e., 20 and 50 TPa^{-1}, respectively. Therefore, the coefficient α is assumed to be equal to zero in this paper. Whether or not the pressure effect can be neglected for a given problem, the main issue in using Eq. (4) is to define ϕ for anisotropic materials.

A tensor denoted by $\tilde{\mathbf{s}}$ can be defined as a linear transformation of **s**, i.e.,

$$\tilde{\mathbf{s}} = \mathbf{C}\mathbf{s} = \mathbf{C}\mathbf{T}\boldsymbol{\sigma} = \mathbf{L}\boldsymbol{\sigma}, \tag{5}$$

where **C** (or **L**) contains constant coefficients and **T** transforms the Cauchy stress tensor $\boldsymbol{\sigma}$ to its deviator **s**. The principal values of $\tilde{\mathbf{s}}$, which define the diagonal tensor representation $\tilde{\mathbf{S}}$, are the roots of the characteristics equation

$$P(\tilde{S}_k) = -\tilde{S}_k^3 + 3H_1\tilde{S}_k^2 + 3H_2\tilde{S}_k + 2H_3 = 0, \tag{6}$$

where the associated 1st, 2nd and 3rd invariants of $\tilde{\mathbf{s}}$ are

$$\begin{aligned}
&\text{(a)} \quad H_1 = (\tilde{s}_{xx} + \tilde{s}_{yy} + \tilde{s}_{zz})/3,\\
&\text{(b)} \quad H_2 = \left(\tilde{s}_{yz}^2 + \tilde{s}_{zx}^2 + \tilde{s}_{xy}^2 - \tilde{s}_{yy}\tilde{s}_{zz} - \tilde{s}_{zz}\tilde{s}_{xx} - \tilde{s}_{xx}\tilde{s}_{yy}\right)/3,\\
&\text{(c)} \quad H_3 = \left(2\tilde{s}_{yz}\tilde{s}_{zx}\tilde{s}_{xy} + \tilde{s}_{xx}\tilde{s}_{yy}\tilde{s}_{zz} - \tilde{s}_{xx}\tilde{s}_{yz}^2 - \tilde{s}_{yy}\tilde{s}_{zx}^2 - \tilde{s}_{zz}\tilde{s}_{xy}^2\right)/2.
\end{aligned} \tag{7}$$

The roots of Eq. (6) are given in Appendix A. Based on this linear transformation, an anisotropic yield function is simply defined by substituting $\tilde{\mathbf{S}}$ for $\mathbf{S}$ in Eq. (3). This yield function keeps its isotropic character if $\mathbf{C}$, the matrix containing the anisotropy coefficients, corresponds to the identity tensor. Because of the linearity of the tensor transformation, the anisotropic yield function is convex if $\phi = \phi(\tilde{\mathbf{S}}) = \phi(\tilde{S}_1, \tilde{S}_2, \tilde{S}_3)$ is convex with respect to its arguments (see previous section). The associated flow rule is used to obtain the strain increments as

$$\mathrm{d}\varepsilon_{ij} = \mathrm{d}\lambda \frac{\partial \phi}{\partial \sigma_{ij}} = \mathrm{d}\lambda \frac{\partial \phi}{\partial \tilde{S}_p} \frac{\partial \tilde{S}_p}{\partial H_q} \frac{\partial H_q}{\partial \tilde{s}_{rs}} \frac{\partial \tilde{s}_{rs}}{\partial \sigma_{ij}}, \tag{8}$$

where $\mathrm{d}\lambda$ is a multiplication factor and the other terms are given in Appendix A.

Instead of one linear transformation, k linear transformations can be considered in order to increase the number of anisotropy coefficients in the formulation

$$\phi = \phi\left(\tilde{\mathbf{S}}^{(1)}, \tilde{\mathbf{S}}^{(2)}, \ldots, \tilde{\mathbf{S}}^{(k)}\right) = h(\bar{\varepsilon}). \tag{9}$$

For instance, for plane stress and full stress states, respectively, Barlat et al. (2003) and Bron and Besson (2004) proposed the following yield condition

$$\phi = \sum_k \phi^{(k)}\left(\tilde{\mathbf{S}}^{(k)}\right) = \bar{\sigma}^a, \tag{10}$$

which defines the effective stress $\bar{\sigma}$. Practically, both conditions were further developed with $k = 2$. For the purpose of clarity, all the subsequent equations will be derived with two linear transformations. Generalization to more linear transformations is possible but two will be sufficient in this work. The two tensors considered are

$$\begin{aligned} &\text{(a)} \quad \tilde{\mathbf{s}}' = \mathbf{C}'\mathbf{s} = \mathbf{C}'\mathbf{T}\boldsymbol{\sigma} = \mathbf{L}'\boldsymbol{\sigma}, \\ &\text{(b)} \quad \tilde{\mathbf{s}}'' = \mathbf{C}''\mathbf{s} = \mathbf{C}''\mathbf{T}\boldsymbol{\sigma} = \mathbf{L}''\boldsymbol{\sigma}. \end{aligned} \tag{11}$$

The yield function must be an isotropic function of its six arguments

$$\phi = \phi(\boldsymbol{\Sigma}) = \phi\left(\tilde{\mathbf{S}}', \tilde{\mathbf{S}}''\right) = \phi\left(\tilde{S}'_1, \tilde{S}'_2, \tilde{S}'_3, \tilde{S}''_1, \tilde{S}''_2, \tilde{S}''_3\right). \tag{12}$$

The principal values of the tensor $\tilde{\mathbf{s}}'$ or $\tilde{\mathbf{s}}''$ are the roots of their respective characteristic equation (6). The anisotropic yield function is convex if ϕ is a convex function of its six arguments (see Appendix A). The gradient of the potential ϕ needed for the associated flow rule is given by

$$\frac{\partial \phi}{\partial \sigma_{ij}} = \frac{\partial \phi}{\partial \tilde{S}'_p} \frac{\partial \tilde{S}'_p}{\partial H'_q} \frac{\partial H'_q}{\partial \tilde{s}'_{rs}} \frac{\partial \tilde{s}'_{rs}}{\partial \sigma_{ij}} + \frac{\partial \phi}{\partial \tilde{S}''_p} \frac{\partial \tilde{S}''_p}{\partial H''_q} \frac{\partial H''_q}{\partial \tilde{s}''_{rs}} \frac{\partial \tilde{s}''_{rs}}{\partial \sigma_{ij}}, \tag{13}$$

where the different terms of the above expression are given in Appendix A.

3. Input data and analysis

Many issues have been addressed in determining yield surfaces experimentally. For instance, the definition of yield has been the subject of discussion (Paul, 1968; Hecker, 1976). In this work, yield is defined conventionally at a certain offset of plastic strain (e.g., 0.2%) and cyclic loading is not considered. Multiaxial experiments have been used to characterize a yield surface (see Hecker, 1976, for a review). However, multiaxial testing is tedious, difficult to perform and interpret, and not suitable for quick characterization of anisotropy. This is more a technique for careful verifications of concepts and theories. Therefore, other methods are necessary to identify material coefficients in constitutive equations, in particular for sheet materials.

Although the yield functions introduced in this work can be used for a general stress state (3D) and any type of forming process, the remainder of this paper will be more concerned with sheet forming applications. Anisotropic properties can be assessed by performing uniaxial tension tests in the **x** and **y** axes (rolling and transverse directions, respectively), and in directions at ξ degrees with respect to **x**. The balanced biaxial yield stress (σ_b) is an important parameter to measure. This stress can be obtained by conducting a hydraulic bulge test (Young et al., 1981). This test is interesting not only because it gives information on the yield surface but also because it provides a measure of the hardening behavior up to strains of about twice those that can be achieved in uniaxial tension. However, the yield stress point is not well defined in this test because of the low curvature of the specimen in the initial stage of deformation.

Because the biaxial stress state in the bulge test is not exactly balanced and the yield locus curvature is usually high around this stress state, measures of the corresponding strain state can lead to substantial errors. However, Barlat et al. (2003) proposed the disk compression test, which gives a measure of the flow anisotropy for a balanced biaxial stress state, assuming that hydrostatic pressure has no influence on plastic deformation. In this test, a 12.7 mm disk is compressed through the normal direction (ND) of the sheet. The strains measured in the **x** and **y** directions lead to a linear relationship in which the slope $(d\varepsilon^p_{yy}/d\varepsilon^p_{xx})$ is denoted by r_b by analogy to the r value in uniaxial tension. This parameter is a direct measure of the slope of the yield locus at the balanced biaxial stress state. Bourne and Hill (1950) reported results obtained with a similar test conducted on a brass sheet sample.

Although the tests described above and other experimental procedures are available to test materials in different stress states, it is not always possible to probe all of them. In this case, microstructure modeling can be used to replace the missing experimental data. The resistance to shear through the thickness of a sheet is not readily available from mechanical experiments. However, crystal plasticity with a measure of the crystallographic texture of the sheet can be used to compute a pseudo-experimental value. Without texture or any other microstructural information available, the out-of-plane properties can be assumed to be equal, as a first approximation, to the isotropic values.

Two separate aspects have to be considered in developing the material constitutive behavior (Barlat et al., 2002). First, one must develop mathematical formulations for yield functions, flow rules and hardening laws, which are appropriate for the class of materials studied and obey physical and mechanical principles. Second, one must analyze the tests and determine the data that best describe the material properties to identify the constitutive parameters. For instance, the yield stresses can be used as input data to calculate the anisotropic yield function coefficients. However, as mentioned above, the yield stress from the bulge test is not very accurate. Moreover, any stress at yield is determined in the region of the stress–strain curve where the slope is the steepest, which might involve additional inaccuracy. Finally, the yield stress is associated with a very small plastic strain and might not reflect the anisotropy of the material at larger strains. For these reasons, the flow stresses at equal amount of plastic work along different loading paths could be selected as input data instead of the yield stress. For many aluminum alloys, experimental observations show that after a few percent plastic strain, the flow stress anisotropy does not vary significantly.

Similar observations are applicable for r values, which can be defined as instantaneous quantities at yield or as the standard slope of the width strain–thickness strain curve over a given deformation range in tension. On one hand, the yield stresses and instantaneous r values at yield are more appropriate to define the coefficients of the yield function. On the other hand, stresses (called flow stresses) defined at a given amount of plastic work and standard r values can characterize the average behavior of the material over a finite deformation range. These values might be more suitable and more descriptive of the average response of the material for sheet forming simulations. In this case, a more appropriate terminology would be flow function and flow surface instead of yield function and yield surface although, mathematically, yield or flow functions are identical concepts.

4. Yield function Yld2004-18p

When large numbers of experimental data are available, typically, uniaxial tension data for seven test directions between the rolling (RD or **x**) and transverse (TD or **y**) directions, as well as balanced biaxial data, the following analytical yield function ϕ, denoted Yld2004-18p, is proposed

$$\begin{aligned}\phi &= \phi(\boldsymbol{\Sigma}) = \phi\left(\tilde{\mathbf{S}}', \tilde{\mathbf{S}}''\right)\\ &= \left|\tilde{S}'_1 - \tilde{S}''_1\right|^a + \left|\tilde{S}'_1 - \tilde{S}''_2\right|^a + \left|\tilde{S}'_1 - \tilde{S}''_3\right|^a + \left|\tilde{S}'_2 - \tilde{S}''_1\right|^a + \left|\tilde{S}'_2 - \tilde{S}''_2\right|^a\\ &\quad + \left|\tilde{S}'_2 - \tilde{S}''_3\right|^a + \left|\tilde{S}'_3 - \tilde{S}''_1\right|^a + \left|\tilde{S}'_3 - \tilde{S}''_2\right|^a + \left|\tilde{S}'_3 - \tilde{S}''_3\right|^a = 4\bar{\sigma}^a. \end{aligned} \tag{14}$$

The associated linear transformations on the stress deviator are

$$\mathbf{C}' = \begin{bmatrix} 0 & -c'_{12} & -c'_{13} & 0 & 0 & 0 \\ -c'_{21} & 0 & -c'_{23} & 0 & 0 & 0 \\ -c'_{31} & -c'_{32} & 0 & 0 & 0 & 0 \\ 0 & 0 & 0 & c'_{44} & 0 & 0 \\ 0 & 0 & 0 & 0 & c'_{55} & 0 \\ 0 & 0 & 0 & 0 & 0 & c'_{66} \end{bmatrix},$$

$$\mathbf{C}'' = \begin{bmatrix} 0 & -c''_{12} & -c''_{13} & 0 & 0 & 0 \\ -c''_{21} & 0 & -c''_{23} & 0 & 0 & 0 \\ -c''_{31} & -c''_{32} & 0 & 0 & 0 & 0 \\ 0 & 0 & 0 & c''_{44} & 0 & 0 \\ 0 & 0 & 0 & 0 & c''_{55} & 0 \\ 0 & 0 & 0 & 0 & 0 & c''_{66} \end{bmatrix}. \tag{15}$$

This is an isotropic and convex function with respect to its arguments (see Appendix A). The two linear transformations provide 18 coefficients that can be used to capture the material anisotropy. When the coefficients are all equal to one, this function reduces to Hershey's isotropic yield function (1954) proposed to reproduce the yield surface calculated with a self-consistent polycrystal model. Based on crystal plasticity, Hosford (1972) and Logan and Hosford (1980) showed that in order to describe the behavior of BCC and FCC materials, the exponent "a" should be 6 and 8, respectively. When $a = 2$ (or 4) and all the coefficients c'_{ij} and c''_{ij} are equal to 1, the yield function reduces to von Mises. In order to determine the coefficients for anisotropic materials, an error function is minimized. A similar approach was proposed by Banabic et al. (2003). In the present work, the error function is defined as

$$E\left(c'_{ij}, c''_{ij}\right) = \sum_p w_p \left(\frac{\sigma_p^{\mathrm{pr}}}{\sigma_p^{\mathrm{ex}}} - 1\right)^2 + \sum_q w_q \left(\frac{r_q^{\mathrm{pr}}}{r_q^{\mathrm{ex}}} - 1\right)^2, \tag{16}$$

where p represents the number of experimental flow stresses and q represents the number of experimental r values available. In the above equation, the superscript denotes whether the corresponding value is experimental or predicted. Each term in the error function is weighted by w (see Appendix A for more details). The coefficients c'_{ij} and c''_{ij} are varied using the steepest descent method in order to minimize the function $E(c'_{ij}, c''_{ij})$.

Note that when $\mathbf{C}'' = \mathbf{C}'$ (or $\mathbf{L}'' = \mathbf{L}'$), i.e., when the formulation accounts for only one linear transformation, Yld2004-18p reduces to Yld91 (Barlat et al., 1991) provided that the number of independent coefficients is imposed to be 6, for instance, c'_{12}, c'_{23}, c'_{31}, c'_{44}, c'_{55} and c'_{66}. Assuming that the linear transformation in Yld91 is represented by $\mathbf{L}$ in Eq. (5) such that

$$\mathbf{L} = \frac{1}{3}\begin{bmatrix} \bar{b}+\bar{c} & -\bar{c} & -\bar{b} & 0 & 0 & 0 \\ -\bar{c} & \bar{c}+\bar{a} & -\bar{a} & 0 & 0 & 0 \\ -\bar{b} & -\bar{a} & \bar{a}+\bar{b} & 0 & 0 & 0 \\ 0 & 0 & 0 & 3\bar{f} & 0 & 0 \\ 0 & 0 & 0 & 0 & 3\bar{g} & 0 \\ 0 & 0 & 0 & 0 & 0 & 3\bar{h} \end{bmatrix}, \tag{17}$$

the symmetry of $\mathbf{L}$ leads to the following constraints on $\mathbf{C}'$

$$\begin{aligned} &\text{(a)} \quad 3c'_{13} = 2c'_{31} + 2c'_{12} - c'_{23}, \\ &\text{(b)} \quad 3c'_{32} = 2c'_{23} + 2c'_{31} - c'_{12}, \\ &\text{(c)} \quad 3c'_{21} = 2c'_{12} + 2c'_{23} - c'_{31}, \end{aligned} \tag{18}$$

and the Yld91 coefficients are given by

$$\begin{aligned} &\text{(a)} \quad \bar{a} = \left(4c'_{23} + c'_{31} - 2c'_{12}\right)/3, \\ &\text{(b)} \quad \bar{b} = \left(4c'_{31} + c'_{12} - 2c'_{23}\right)/3, \\ &\text{(c)} \quad \bar{c} = \left(4c'_{12} + c'_{23} - 2c'_{31}\right)/3, \\ &\text{(d)} \quad \bar{f} = c'_{44}, \\ &\text{(e)} \quad \bar{g} = c'_{55}, \\ &\text{(f)} \quad \bar{h} = c'_{66}. \end{aligned} \tag{19}$$

For sheet forming applications, the experimental data in the error function consists of flow stresses and r values for tension in seven directions in the plane of the sheet (RD to TD in 15° increments for instance), the biaxial flow stress from the bulge test and the biaxial r value from the disk compression test (r_b). If r_b is

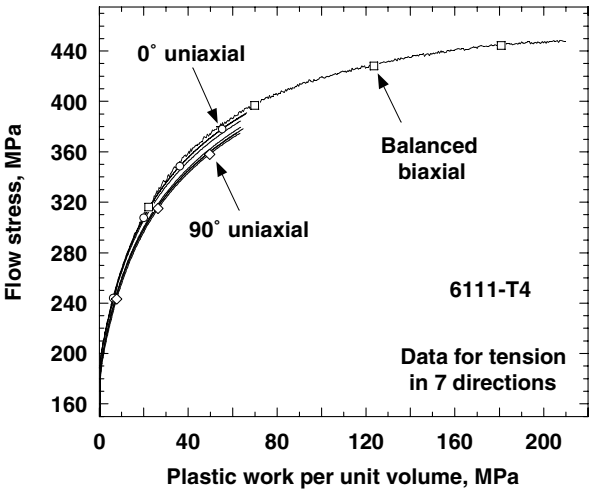

Fig. 1. Uniaxial and biaxial (bulge test) flow stresses as a function of plastic work per unit volume.

not available experimentally, it can be computed from another yield function (Barlat et al., 1997) by solving an implicit non-linear system of five equations (see Appendix A). Moreover, four additional data characterizing out-of-plane properties are also needed in the error function. Because no simple experiments can give the properties for the *yz* and *zx* stress components, polycrystal simulations were performed to provide the yield stress for simple shear in the **yz** and **zx** planes and uniaxial tension at 45° between **y** and **z**, and between **z** and **x**. Here, **z** (or ND) denotes the sheet normal direction. When crystallographic texture is not available, it is recommended to set the out-of-plane properties to their isotropic values, i.e., $\sigma/\bar{\sigma} = 1$ for tension and $\tau/\bar{\sigma} = 1/(1+2^{a-1})^{1/a}$ for simple shear.

The first application example of Yld2004-18p pertains to a mildly anisotropic 6111-T4 aluminum alloy sheet sample. The balanced biaxial tension stress–strain curve was obtained using the bulge test (Young et al., 1981). Fig. 1 illustrates the balanced biaxial and the different tensile flow stresses as a function of plastic work. This figure shows that the anisotropic behavior of the material is constant over the useful strain range indicating that isotropic hardening is a very reasonable assumption. Fig. 2 shows the results of the disk compression test as well as selected specimens after different amounts of deformation. The good linear regression indicates that the slope

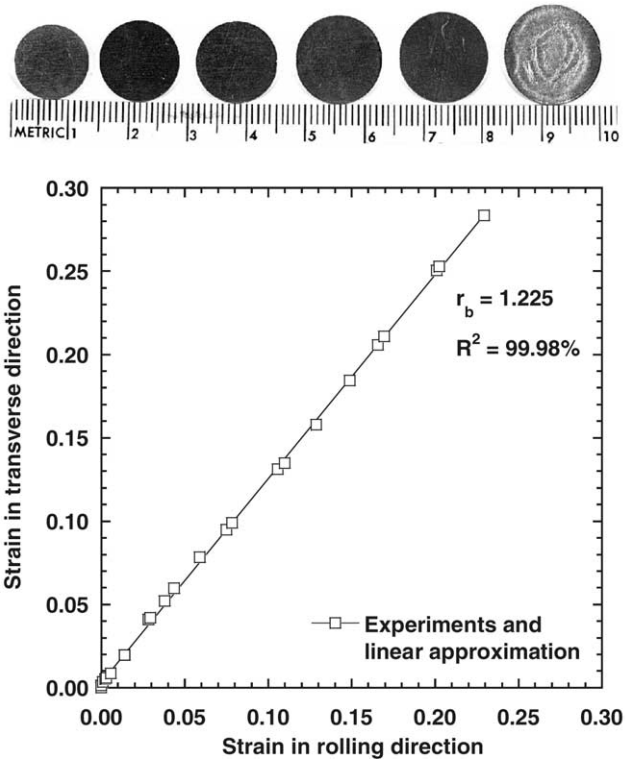

Fig. 2. TD vs. RD strains measured on the specimen during the disk compression test for 6111-T4.

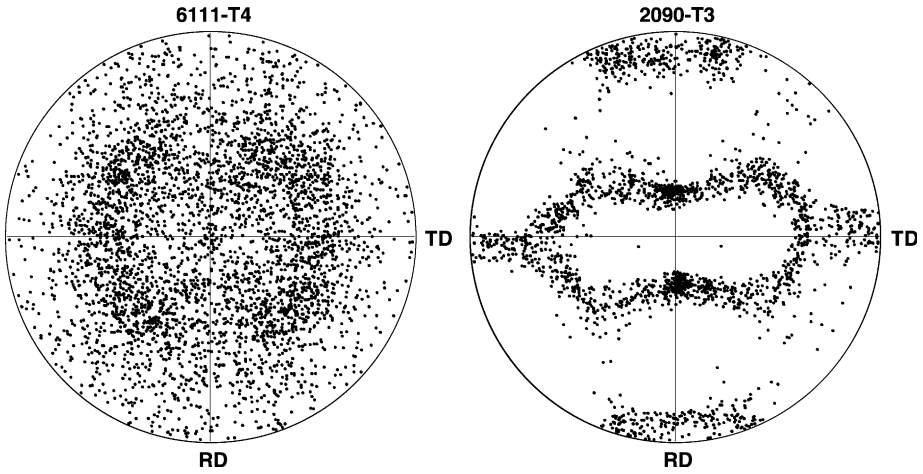

Fig. 3. (1 1 1) pole figures for 6111-T4 and 2090-T3.

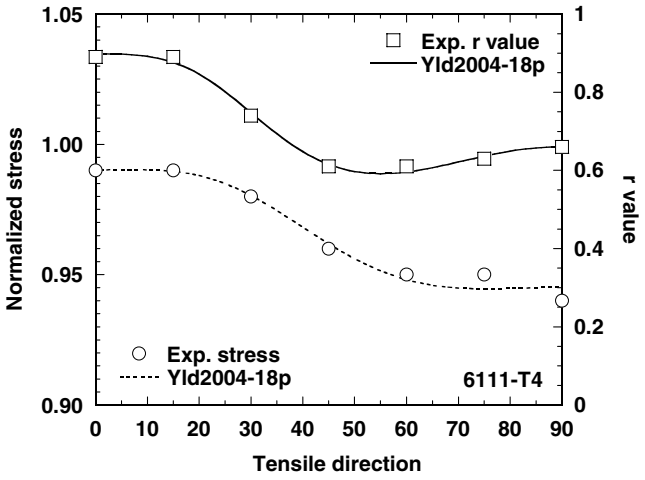

Fig. 4. Anisotropy of the flow stress (normalized by the biaxial flow stress) and the r value for 6111-T4, measured and calculated with Yld2004-18p.

of the yield surface at the balanced biaxial stress state remains the same as deformation proceeds. The mild crystallographic texture of 6111-T4, represented as a (1 1 1) pole figure (Fig. 3), was used as input to the VPSC polycrystal model (Lebensohn and Tomé, 1993) to compute the out-of-plane material properties.

Fig. 4 compares experimental and calculated uniaxial flow properties, i.e., normalized flow stresses and r values as a function of the tensile direction (angle from RD). Since all of these data were used to identify the coefficients, the calculations are not really predictive. However, the main point of these curves is to demonstrate

Table 1
Out-of-plane uniaxial and simple shear flow stresses for 6111-T4 and 2090-T3

	Model	*yz* 45° tension	*zx* 45° tension	*yz* simple shear	*zx* simple shear
6111-T4	VPSC polycrystal	1.07	1.04	0.67	0.65
	Yld2004-18p	1.07	1.04	0.67	0.65
	Yld2004-13p	1.10	1.08	0.63	0.60
2090-T3	VPSC polycrystal	0.90	0.89	0.47	0.47
	Yld2004-18p	0.85	0.87	0.52	0.49
	Yld2004-13p	0.90	0.89	0.46	0.47

that the model is flexible enough to describe the whole set of anisotropic data (*r* values and flow stresses) simultaneously. The yield function must describe at least tensile anisotropy accurately if its extrapolation to any other stress state has a reasonable chance to capture the material behavior. This flexibility cannot be achieved with models that are based on one linear transformation only. Table 1 gives the values of the *yz* and *zx* mechanical properties predicted with the polycrystal model and with Yld2004-18p. The agreement between these two sets of data is excellent. Finally, Fig. 5 shows the yield surface of 6111-T4 represented as contours of the normalized shear stress $\sigma_{xy}/\bar{\sigma}$ projected onto the normal stress plane $(\sigma_{xx}/\bar{\sigma},\ \sigma_{yy}/\bar{\sigma})$. The circles correspond to the projection onto this plane of the experimental flow stresses used for the identification of the anisotropy coefficients. For instance, for uniaxial

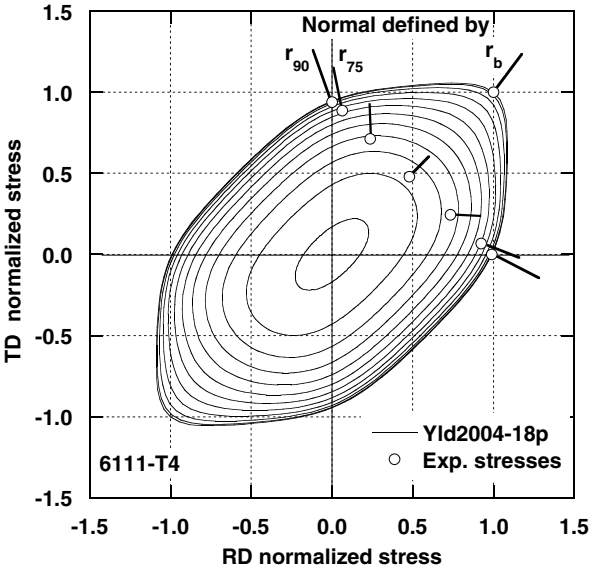

Fig. 5. Yld2004-18p yield surface represented by contours of normalized shear in 0.05 increments from 0, and projection of experimental data for 6111-T4. The experimental data shown here represent the physical parameters controlling the yield surface shape. The coefficients c'_{ij} and c''_{ij} have no real physical meaning.

Table 2
Yld2004-18p and Yld2004-13p coefficients for 6111-T4 and 2090-T3 (exponent $a = 8$)

	Yld2004-18p		Yld2004-13p	
	6111-T4	2090-T3	6111-T4	2090-T3
c'_{12}	1.241024	−0.069888	1.000000	1.000000
c'_{13}	1.078271	0.936408	−0.056873	−0.610193
c'_{21}	1.216463	0.079143	1.007956	0.835890
c'_{23}	1.223867	1.003060	−0.044674	−0.092134
c'_{31}	1.093105	0.524741	1.000000	1.000000
c'_{32}	0.889161	1.363180	1.000000	1.000000
c'_{44}	0.501909	1.023770	0.865703	1.177300
c'_{55}	0.557173	1.069060	0.900304	1.165140
c'_{66}	1.349094	0.954322	0.980803	1.228700
c''_{12}	0.775366	0.981171	0.934338	1.154650
c''_{13}	0.922743	0.476741	0.765452	0.899502
c''_{21}	0.765487	0.575316	1.225251	1.383330
c''_{23}	0.793356	0.866827	0.653728	0.568485
c''_{31}	0.918689	1.145010	1.000000	1.000000
c''_{32}	1.027625	−0.079294	1.000000	1.000000
c''_{44}	1.115833	1.051660	1.058472	1.001980
c''_{55}	1.112273	1.147100	1.008556	1.001050
c''_{66}	0.589787	1.404620	1.198512	1.488390

tension at 45° from the RD with flow stress σ_{45}, the stress components are $\sigma_{xy} = \sigma_{yy} = \sigma_{xx} = \sigma_{45}/2$. The lines represent the projected direction normal to the yield surface at these points. These directions can be calculated from the corresponding r values. The coefficients of this particular yield function are listed in Table 2.

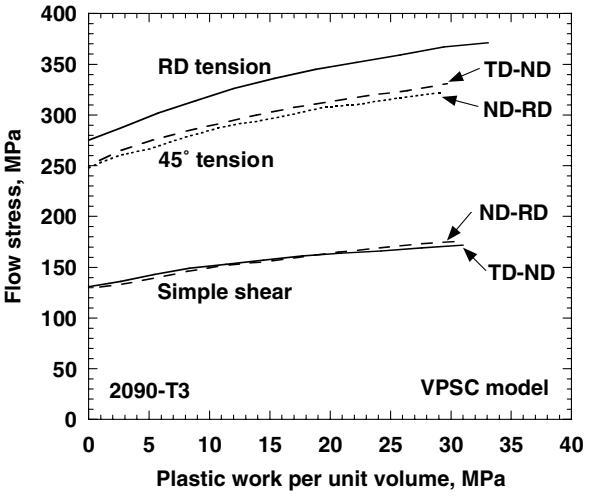

Fig. 6. Flow stress vs. plastic work curves in RD tension, 45° tension in the TD–ND plane, 45° tension in the TD–ND plane, simple shear in the TD–ND plane and simple shear in the ND–RD plane for 2090-T3.

In the second example, Yld2004-18p is applied to a strongly anisotropic 2090-T3 aluminum alloy sheet sample. The anisotropy of this material can be associated to its strong crystallographic texture (Fig. 3). Fig. 6 shows the flow stress of this material as a function of the plastic work for different applied boundary conditions as predicted with the VPSC model. These curves were used to evaluate the out-of-plane properties of the 2090-T3 sheet. Together with the experimental in-plane properties, they were used as input data for the calculation of the yield function coefficients, which are given in Table 2. Fig. 7 shows that the anisotropy of the tensile properties is very well captured by the model. The variation in r values with six peaks between 0° and 360° indicates that this model is likely to be suitable for the prediction of six or more ears in cups drawn from circular blanks. Table 1 shows the values of the yz and zx mechanical properties predicted with the polycrystal model and with Yld2004-18p. The agreement between the two sets of data is not as good for this material as compared to 6111-T4. However, since the properties in the plane are more important for sheet forming applications, the anisotropy coefficients were optimized with a smaller weight for the yz and zx properties (see Appendix A on the error function). Moreover, because this material exhibits a very strong crystallographic texture gradient (Barlat et al., 1991), the crystal plasticity predictions might not have been as accurate as desired. Figs. 8–10 present the yield surfaces represented as contours of the normalized shear stresses for three possible plane stress states, i.e., in the **xy**, **yz** and **zx** planes, respectively. These figures illustrate the high distortion of the yield surface for this 2090-T3 sheet sample.

When a limited number of experimental data are available, the plane stress function Yld2000-2d (Barlat et al., 2003) can be used to generate additional flow stresses,

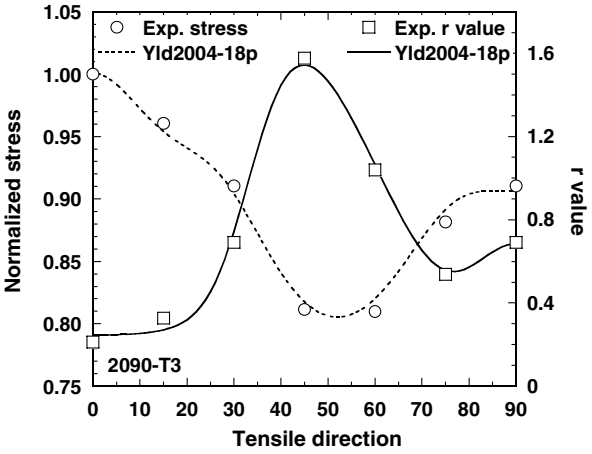

Fig. 7. Anisotropy of the flow stress (normalized by the RD uniaxial flow stress) and the r value for 2090-T3, measured and calculated with Yld2004-18p.

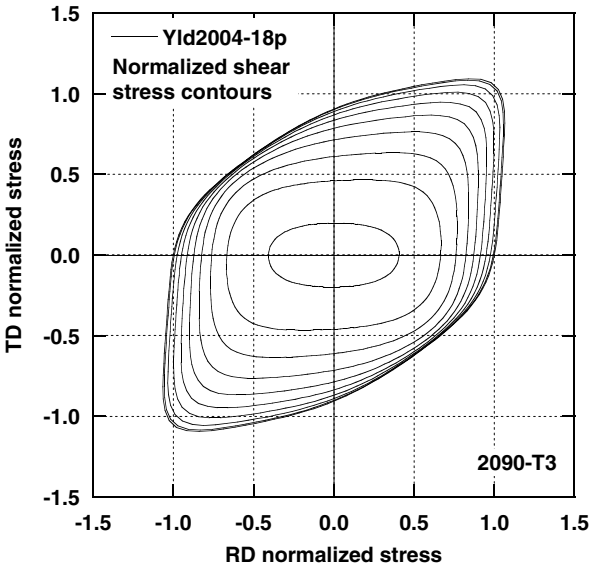

Fig. 8. Yld2004-18 yield surface represented by contours of normalized shear in 0.05 increments from 0 for plane stress in the RD–TD plane for 2090-T3.

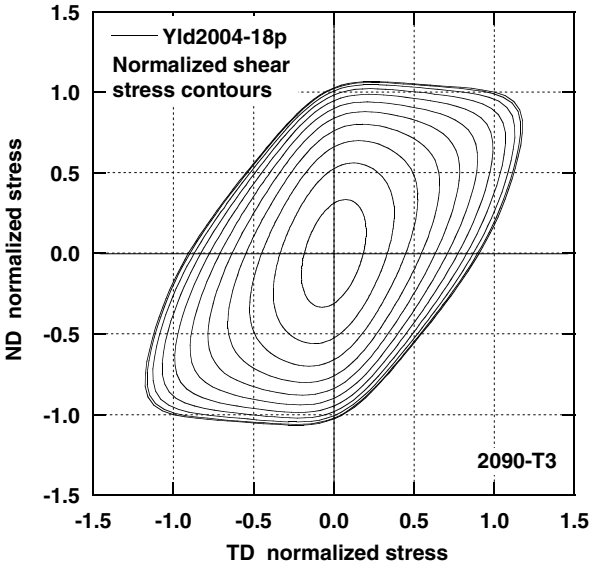

Fig. 9. Yld2004-18p yield surface represented by contours of normalized shear in 0.05 increments from 0 for plane stress in the TD–ND plane for 2090-T3.

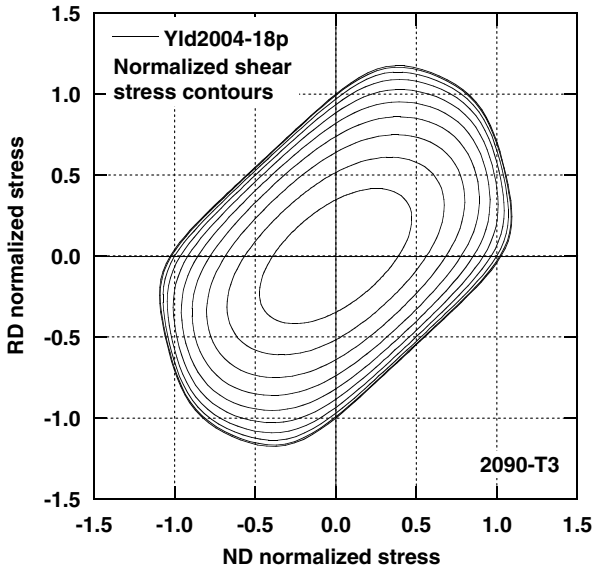

Fig. 10. Yld2004-18p yield surface represented by contours of normalized shear in 0.05 increments from 0 for plane stress in the ND–RD plane for 2090-T3.

r values or yield locus data. Then, both data, experimentally measured and calculated with Yld20002-d, can be used in the error function to compute the Yld2004-18p coefficients. An alternate approach is to use another yield function, Yld2004-13p, which is described in the next section.

5. Yield function Yld2004-13p

In this yield function, the isotropic formulation differs from that of the previous section

$$\begin{aligned}\phi &= \phi'\left(\tilde{\mathbf{S}}'\right) + \phi''\left(\tilde{\mathbf{S}}''\right)\\ &= \left|\tilde{S}'_1 - \tilde{S}'_2\right|^a + \left|\tilde{S}'_2 - \tilde{S}'_3\right|^a + \left|\tilde{S}'_3 - \tilde{S}'_1\right|^a - \left\{\left|\tilde{S}'_1\right|^a + \left|\tilde{S}'_2\right|^a + \left|\tilde{S}'_3\right|^a\right\} + \left|\tilde{S}''_1\right|^a\\ &\quad + \left|\tilde{S}''_2\right|^a + \left|\tilde{S}''_3\right|^a = 2\bar{\sigma}^a. \end{aligned} \tag{20}$$

Moreover, the general linear transformations are reduced to a total of thirteen coefficients

$$\mathbf{C}' = \begin{bmatrix} 0 & -1 & -c'_{13} & 0 & 0 & 0 \\ -c'_{21} & 0 & -c'_{23} & 0 & 0 & 0 \\ -1 & -1 & 0 & 0 & 0 & 0 \\ 0 & 0 & 0 & c'_{44} & 0 & 0 \\ 0 & 0 & 0 & 0 & c'_{55} & 0 \\ 0 & 0 & 0 & 0 & 0 & c'_{66} \end{bmatrix},$$

$$\mathbf{C}'' = \begin{bmatrix} 0 & -c''_{12} & -c''_{13} & 0 & 0 & 0 \\ -c''_{21} & 0 & -c''_{23} & 0 & 0 & 0 \\ -1 & -1 & 0 & 0 & 0 & 0 \\ 0 & 0 & 0 & c''_{44} & 0 & 0 \\ 0 & 0 & 0 & 0 & c''_{55} & 0 \\ 0 & 0 & 0 & 0 & 0 & c''_{66} \end{bmatrix}. \tag{21}$$

In the isotropic case, it reduces to Hershey's yield function. By visual inspection of the calculated yield locus or by computation of the Hessian matrix for a sufficiently high value of the exponent a (larger than about 1.7), it can be shown that both isotropic functions (ϕ', ϕ''), and therefore their sum, are convex. This combination of linear transformations and yield function was selected because it provides an alternate yield function, which leads to a fast minimization of the error function for a number of materials. This particular formulation is more appropriate for sheet materials and appears to have enough flexibility to capture the anisotropic behavior of many metals and alloys.

It should be mentioned that 13 parameters are necessary in the definition of the matrices $\mathbf{C}'$ and $\mathbf{C}''$ for Yld2004-13p. For plane stress applications, the number of required parameters reduces to nine. Although eight parameters would be sufficient for this case, see for instance (Barlat et al., 2003), a kind of 'locking effect' was observed if only eight parameters (or 12 in the full stress space) were used, i.e., the yield function is then more constrained than in the case where nine parameters are used. This 'locking effect' appears to be due to the fact that, even in plane stress applications, the fit of the yield function to mechanical input data is more difficult with a full stress formulation than with a plane stress formulation (such as in Barlat et al., 2003). In a general 3D framework, however, a full stress state must be accounted for. For this reason, thirteen parameters were introduced in the formulation.

As in the previous section, the computations of the coefficients were performed for the mildly anisotropic 6111-T4 and the strongly anisotropic 2090-T3 sheet samples (see Table 2). Fig. 11 shows the experimental and predicted variations of the flow stresses and r values for 6111-T4. Compared to Fig. 4, little differences can be observed. This is because both Yld2004-13p and Yld2004-18p yield surface shape are very similar in this case. Only the out-of-plane properties differ somewhat from the pseudo-experimental and Yld2004-18p predicted values (Table 1).

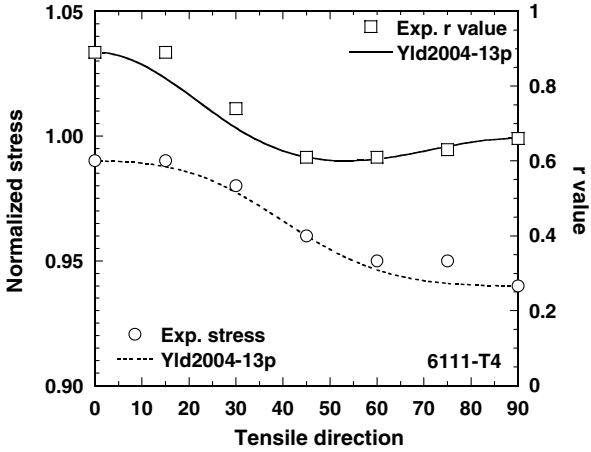

Fig. 11. Anisotropy of the flow stress (normalized by the biaxial flow stress) and the *r* value for 6111-T4, measured and predicted with Yld2004-13p.

Fig. 12 shows the experimental and predicted anisotropic properties of the 2090-T3 sheet sample. In this case, the experimental anisotropy is not predicted as accurately as with Yld2004-18p. However, the main experimental trends are well captured at a level of accuracy similar to that obtained with Yld2000-2d (Barlat et al., 2003). Moreover, perhaps coincidentally, the out-of-plane pseudo-experimental data are well predicted with Yld2004-13p (Table 1). Finally, Fig. 13 presents the yield surfaces represented as contours of the normalized shear stresses in the **xy** plane

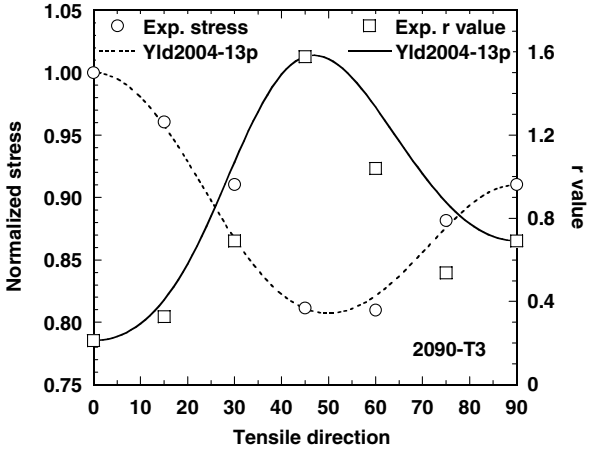

Fig. 12. Anisotropy of the flow stress (normalized by the RD uniaxial flow stress) and the *r* value for 2090-T3, measured and predicted with Yld2004-13p.

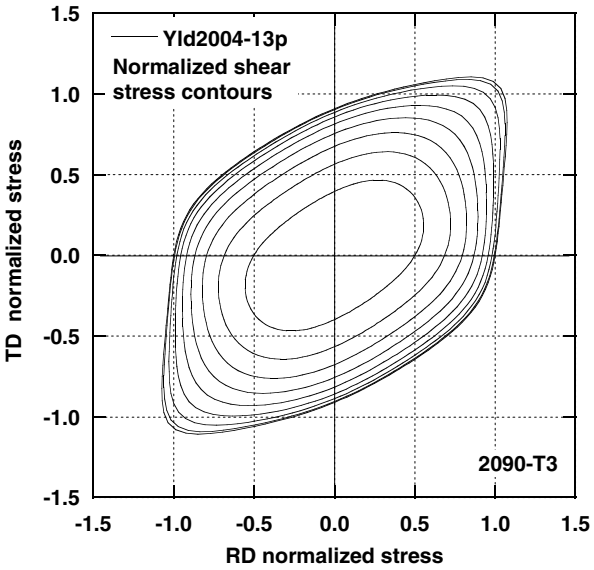

Fig. 13. Yld2004-13p yield surface represented by contours of normalized shear in 0.05 increments from 0 for plane stress in the RD–TD plane for 2090-T3.

for the 2090-T3 sheet sample. The contour corresponding to $\sigma_{xy}/\bar{\sigma} = 0$, i.e., the usual yield locus, is similar to that of Yld2004-18p represented in Fig. 8. However, in general, the contours of constant normalized shear stresses are not identical for the two models, reflecting the ability of Yld2004-18p to describe the uniaxial plastic properties for tensile axes away from **x** and **y** with more accuracy.

6. Conclusions

In this paper, yield functions describing the anisotropic behavior of metals and alloys in the full stress space are proposed. Both functions are based on two linear transformations of the stress deviator. These functions are convex and are expected to lead to successful 3D finite element simulations of forming processes or any computations involving anisotropic plasticity.

The first yield function contains 18 parameters and can describe the anisotropic properties, flow stresses and r values in uniaxial tension of sheet materials very accurately. As a result, this function is expected to predict at least six ears in the deep drawing simulations of circular blanks.

The second function, Yld2004-13p, contains 13 parameters and does not require as much experimental data compared to Yld2004-18p for the determination of its coefficients. As a result, it cannot reproduce all details of the tensile flow stress and r value anisotropy in sheet samples, but it provides a very reasonable description of the main trends.

Acknowledgements

The authors would like to thank Dr. C. Tomé from the Los Alamos National Laboratory, USA, for providing and supporting the use of the VPSC code. The authors are grateful to Pr. K. Chung, Seoul National University, Korea, and Dr. L.A. Lalli, Alcoa Technical Center, USA, for their suggestions on the manuscript.

Appendix A. Yield function and derivatives

A.1. Yield function formulations

The anisotropic 3D (6 stress components) yield function operates on six arguments formally represented by the column matrix of these arguments $\boldsymbol{\Sigma} = [\tilde{S}'_1, \tilde{S}'_2, \tilde{S}'_3, \tilde{S}''_1, \tilde{S}''_2, \tilde{S}''_3]^{\mathrm{T}}$

$$\phi = \phi(\boldsymbol{\Sigma}) = \phi(\tilde{\mathbf{S}}', \tilde{\mathbf{S}}'') = \phi\left(\tilde{S}'_i, \tilde{S}''_j\right) = \phi\left(\tilde{S}'_1, \tilde{S}'_2, \tilde{S}'_3, \tilde{S}''_1, \tilde{S}''_2, \tilde{S}''_3\right), \tag{A.1}$$

$\tilde{S}'_i$ and $\tilde{S}''_j$ are the principal values of the tensors $\tilde{\mathbf{s}}'$ and $\tilde{\mathbf{s}}''$ defined by two linear transformations on the stress deviator $\mathbf{s}$

$$\begin{aligned} \tilde{\mathbf{s}}' &= \mathbf{C}'\mathbf{s} = \mathbf{C}'\mathbf{T}\boldsymbol{\sigma} = \mathbf{L}'\boldsymbol{\sigma}, \\ \tilde{\mathbf{s}}'' &= \mathbf{C}''\mathbf{s} = \mathbf{C}''\mathbf{T}\boldsymbol{\sigma} = \mathbf{L}''\boldsymbol{\sigma}, \end{aligned} \tag{A.2}$$

where $\boldsymbol{\sigma}$ is the Cauchy stress tensor. $\mathbf{C}'$ and $\mathbf{C}''$, the matrices containing the anisotropy coefficients, have the form of $\mathbf{C}$ below, and $\mathbf{T}$ transforms the stress tensor to its deviator $\mathbf{s}$

$$\mathbf{C} = \begin{bmatrix} 0 & -c_{12} & -c_{13} & 0 & 0 & 0 \\ -c_{21} & 0 & -c_{23} & 0 & 0 & 0 \\ -c_{31} & -c_{32} & 0 & 0 & 0 & 0 \\ 0 & 0 & 0 & c_{44} & 0 & 0 \\ 0 & 0 & 0 & 0 & c_{55} & 0 \\ 0 & 0 & 0 & 0 & 0 & c_{66} \end{bmatrix} \quad \text{and}$$

$$\mathbf{T} = \frac{1}{3}\begin{bmatrix} 2 & -1 & -1 & 0 & 0 & 0 \\ -1 & 2 & -1 & 0 & 0 & 0 \\ -1 & -1 & 2 & 0 & 0 & 0 \\ 0 & 0 & 0 & 3 & 0 & 0 \\ 0 & 0 & 0 & 0 & 3 & 0 \\ 0 & 0 & 0 & 0 & 0 & 3 \end{bmatrix}. \tag{A.3}$$

For Yld2004-18p and Yld2004-13p, the yield function ϕ and linear transformations ($\mathbf{C}'$ and $\mathbf{C}''$) are given in Sections 4 and 5, respectively. If the tensor $\tilde{\mathbf{s}}$ ($\tilde{\mathbf{s}}'$ or $\tilde{\mathbf{s}}''$), expressed in ($\mathbf{x}$, $\mathbf{y}$, $\mathbf{z}$), is represented by

$$\tilde{\mathbf{s}} = \begin{bmatrix} \tilde{s}_{xx} & \tilde{s}_{xy} & \tilde{s}_{zx} \\ \tilde{s}_{xy} & \tilde{s}_{yy} & \tilde{s}_{yz} \\ \tilde{s}_{zx} & \tilde{s}_{yz} & \tilde{s}_{zz} \end{bmatrix}, \tag{A.4}$$

its principal values are the roots of the characteristic equation

$$P(\tilde{S}_k) = -\tilde{S}_k^3 + 3H_1\tilde{S}_k^2 + 3H_2\tilde{S}_k + 2H_3 = 0. \tag{A.5}$$

The associated 1st, 2nd and 3rd invariants of $\tilde{\mathbf{s}}$ are

$$\begin{aligned} &\text{(a)} \quad H_1 = (\tilde{s}_{xx} + \tilde{s}_{yy} + \tilde{s}_{zz})/3, \\ &\text{(b)} \quad H_2 = \left(\tilde{s}_{yz}^2 + \tilde{s}_{zx}^2 + \tilde{s}_{xy}^2 - \tilde{s}_{yy}\tilde{s}_{zz} - \tilde{s}_{zz}\tilde{s}_{xx} - \tilde{s}_{xx}\tilde{s}_{yy}\right)/3, \\ &\text{(c)} \quad H_3 = \left(2\tilde{s}_{yz}\tilde{s}_{zx}\tilde{s}_{xy} + \tilde{s}_{xx}\tilde{s}_{yy}\tilde{s}_{zz} - \tilde{s}_{xx}\tilde{s}_{yz}^2 - \tilde{s}_{yy}\tilde{s}_{zx}^2 - \tilde{s}_{zz}\tilde{s}_{xy}^2\right)/2. \end{aligned} \tag{A.6}$$

Using the change of variables,

$$\tilde{S}_k = \bar{S}_k + H_1, \tag{A.7}$$

the characteristic equation becomes

$$P(\tilde{S}_k) = P'(\bar{S}_k) = -\bar{S}_k^3 + 3p\bar{S}_k + 2q = 0, \tag{A.8}$$

where P and P' are also stress tensor invariants

$$\begin{aligned} &\text{(a)} \quad p = (H_1^2 + H_2) \geqslant 0, \\ &\text{(b)} \quad q = (2H_1^3 + 3H_1H_2 + 2H_3)/2, \\ &\text{(c)} \quad \theta = \arccos\left[\frac{q}{p^{3/2}}\right]. \end{aligned} \tag{A.9}$$

Cardan's solutions to Eq. (A.8) are

$$\begin{aligned} &\text{(a)} \quad \bar{S}_1 = z^{1/3} + \bar{z}^{1/3}, \\ &\text{(b)} \quad \bar{S}_2 = \omega z^{1/3} + \bar{\omega}\bar{z}^{1/3}, \\ &\text{(c)} \quad \bar{S}_3 = \bar{\omega} z^{1/3} + \omega\bar{z}^{1/3}, \end{aligned} \tag{A.10}$$

where z is complex number, ω is a complex constant ($e^{-2i\pi/3}$), and $\bar{z}$ and $\bar{\omega}$ are their conjugate quantities.

$$z = q + i\sqrt{p^3 - q^2}. \tag{A.11}$$

The principal values of $\tilde{\mathbf{s}}$ are

$$\begin{aligned}
&(a)\quad \tilde{S}_1 = \bar{S}_1 + H_1 = 2\sqrt{H_1^2 + H_2}\cos\left(\frac{\theta}{3}\right) + H_1,\\
&(b)\quad \tilde{S}_2 = \bar{S}_2 + H_1 = 2\sqrt{H_1^2 + H_2}\cos\left(\frac{\theta + 4\pi}{3}\right) + H_1,\\
&(c)\quad \tilde{S}_3 = \bar{S}_3 + H_1 = 2\sqrt{H_1^2 + H_2}\cos\left(\frac{\theta + 2\pi}{3}\right) + H_1.
\end{aligned} \tag{A.12}$$

These values are ordered as shown in Fig. 14, because the argument of $z^{1/3}$ is less than or equal to $\pi/3$.

$$\tilde{S}_1 \geqslant \tilde{S}_2 \geqslant \tilde{S}_3, \quad \tilde{S}_1 > \tilde{S}_3. \tag{A.13}$$

The yield function ϕ is convex (Rockafellar, 1972) in the variables $\tilde{S}'_p, \tilde{S}''_q$ (principal transformed stresses). The tensor transformations, represented by the matrix $\mathbf{q} = [q_{ij}]$, between the principal and non-principal reference frame, lead to

$$\begin{aligned}
&(a)\quad \tilde{\mathbf{S}}' = \mathbf{Q}'\tilde{\mathbf{s}}' = \mathbf{Q}'\mathbf{L}'\boldsymbol{\sigma},\\
&(b)\quad \tilde{\mathbf{S}}'' = \mathbf{Q}''\tilde{\mathbf{s}}'' = \mathbf{Q}''\mathbf{L}''\boldsymbol{\sigma},
\end{aligned} \tag{A.14}$$

where

$$\tilde{\mathbf{S}} = \begin{bmatrix} \tilde{S}_1 \\ \tilde{S}_2 \\ \tilde{S}_3 \end{bmatrix} = \begin{bmatrix} q_{11}^2 & q_{21}^2 & q_{31}^2 & 2q_{21}q_{31} & 2q_{31}q_{11} & 2q_{11}q_{21} \\ q_{12}^2 & q_{22}^2 & q_{32}^2 & 2q_{22}q_{32} & 2q_{32}q_{12} & 2q_{12}q_{22} \\ q_{13}^2 & q_{23}^2 & q_{33}^2 & 2q_{23}q_{33} & 2q_{33}q_{13} & 2q_{13}q_{23} \end{bmatrix} \begin{bmatrix} \tilde{s}_{xx} \\ \tilde{s}_{yy} \\ \tilde{s}_{zz} \\ \tilde{s}_{yz} \\ \tilde{s}_{zx} \\ \tilde{s}_{xy} \end{bmatrix} = \mathbf{Q}\tilde{\mathbf{s}} \tag{A.15}$$

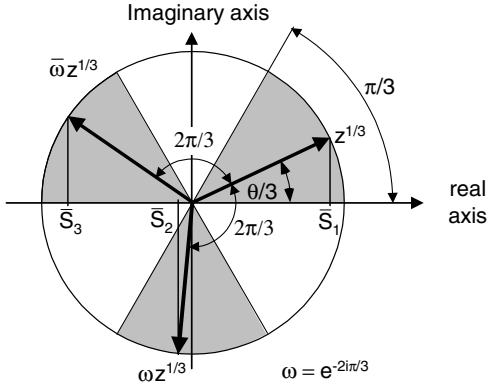

Fig. 14. Stress deviator invariants in complex number space.

for both transformations (prime and double prime). Note that $\mathbf{Q}'\mathbf{L}'$ and $\mathbf{Q}''\mathbf{L}''$ are 3 by 6 matrices. Combining these equations leads to

$$\boldsymbol{\Sigma} = \begin{bmatrix} \tilde{\mathbf{S}}' \\ \tilde{\mathbf{S}}'' \end{bmatrix} = \begin{bmatrix} \mathbf{Q}'\mathbf{L}' \\ \mathbf{Q}''\mathbf{L}'' \end{bmatrix} \boldsymbol{\sigma} \quad \text{or} \quad \boldsymbol{\Sigma} = \boldsymbol{\Theta}\boldsymbol{\sigma}. \tag{A.16}$$

Even if $\boldsymbol{\Theta}$ has no inverse, the above equation shows a linear relationship between the component of $\boldsymbol{\sigma}$ and the arguments of the yield function represented by $\boldsymbol{\Sigma}$. Because a linear transformation on the arguments of a function preserves the convexity, this shows that ϕ is a convex function with respect to the components of the stress tensor $\boldsymbol{\sigma}$.

A.2. Yield function first derivatives

The associated flow rule is used to obtain the strain increments

$$\mathrm{d}\varepsilon_{ij} = \mathrm{d}\lambda \frac{\partial \phi}{\partial \sigma_{ij}}, \tag{A.17}$$

where

$$\begin{aligned} \frac{\partial \phi}{\partial \sigma_{ij}} &= \frac{\partial \phi}{\partial \tilde{S}'_p} \frac{\partial \tilde{S}'_p}{\partial H'_q} \frac{\partial H'_q}{\partial \tilde{s}'_{rs}} \frac{\partial \tilde{s}'_{rs}}{\partial \sigma_{ij}} + \frac{\partial \phi}{\partial \tilde{S}''_p} \frac{\partial \tilde{S}''_p}{\partial H''_q} \frac{\partial H''_q}{\partial \tilde{s}''_{rs}} \frac{\partial \tilde{s}''_{rs}}{\partial \sigma_{ij}} \\ &= \phi'_{,p} S'_{p,q} H'_{q,rs} L'_{rsij} + \phi''_{,p} S''_{p,q} H''_{q,rs} L''_{rsij}. \end{aligned} \tag{A.18}$$

Expressions for $\partial\phi/\partial\tilde{S}_p = \phi_{,p}$ *for Yld2004-18p*

$$\begin{aligned} \text{(a)} \quad \phi'_{,p} &= \frac{\partial \phi}{\partial \tilde{S}'_p} = a\left[\left(\tilde{S}'_p - \tilde{S}''_1\right)\left|\tilde{S}'_p - \tilde{S}''_1\right|^{a-2} + \left(\tilde{S}'_p - \tilde{S}''_2\right)\left|\tilde{S}'_p - \tilde{S}''_2\right|^{a-2}\right. \\ &\quad \left. + \left(\tilde{S}'_p - \tilde{S}''_3\right)\left|\tilde{S}'_p - \tilde{S}''_3\right|^{a-2}\right], \\ \text{(b)} \quad \phi''_{,p} &= \frac{\partial \phi}{\partial \tilde{S}''_p} = -a\left[\left(\tilde{S}'_1 - \tilde{S}''_p\right)\left|\tilde{S}'_1 - \tilde{S}''_p\right|^{a-2} + \left(\tilde{S}'_2 - \tilde{S}''_p\right)\left|\tilde{S}'_2 - \tilde{S}''_p\right|^{a-2}\right. \\ &\quad \left. + \left(\tilde{S}'_3 - \tilde{S}''_p\right)\left|\tilde{S}'_3 - \tilde{S}''_p\right|^{a-2}\right]. \end{aligned} \tag{A.19}$$

Expressions for $\partial S_p/\partial H_q = S_{p,q}$

Differentiating Eq. (A.5) leads to

$$\begin{aligned} \text{(a)} \quad & \frac{\partial \tilde{S}_p}{\partial H_1} = \frac{\tilde{S}_p^2}{\tilde{S}_p^2 - 2H_1\tilde{S}_p - H_2}, \\ \text{(b)} \quad & \frac{\partial \tilde{S}_p}{\partial H_2} = \frac{\tilde{S}_p}{\tilde{S}_p^2 - 2H_1\tilde{S}_p - H_2}, \\ \text{(c)} \quad & \frac{\partial \tilde{S}_p}{\partial H_3} = \frac{2}{3\left(\tilde{S}_p^2 - 2H_1\tilde{S}_p - H_2\right)}. \end{aligned} \tag{A.20}$$

Expressions for $\partial H_q/\partial \tilde{s}_{ij} = H_{q,rs}$

$$
\begin{aligned}
&\text{(a)} \quad \frac{\partial H_1}{\partial \tilde{s}_{xx}} = 1/3, \quad \frac{\partial H_1}{\partial \tilde{s}_{yy}} = 1/3, \quad \frac{\partial H_1}{\partial \tilde{s}_{zz}} = 1/3 \quad \text{and} \quad \frac{\partial H_1}{\partial \tilde{s}_{rs}} = 0 \qquad \text{if } r \neq s,\\
&\text{(b)} \quad \frac{\partial H_2}{\partial \tilde{s}_{xx}} = -\left(\tilde{s}_{yy} + \tilde{s}_{zz}\right)/3, \quad \frac{\partial H_2}{\partial \tilde{s}_{yy}} = -\left(\tilde{s}_{zz} + \tilde{s}_{xx}\right)/3, \quad \frac{\partial H_2}{\partial \tilde{s}_{zz}} = -\left(\tilde{s}_{xx} + \tilde{s}_{yy}\right)/3,\\
&\text{(c)} \quad \frac{\partial H_2}{\partial \tilde{s}_{yz}} = 2\tilde{s}_{yz}/3, \quad \frac{\partial H_2}{\partial \tilde{s}_{zx}} = 2\tilde{s}_{zx}/3, \quad \frac{\partial H_2}{\partial \tilde{s}_{xy}} = 2\tilde{s}_{xy}/3,\\
&\text{(d)} \quad \frac{\partial H_3}{\partial \tilde{s}_{xx}} = \left(\tilde{s}_{yy}\tilde{s}_{zz} - \tilde{s}_{yz}^2\right)/2, \quad \frac{\partial H_3}{\partial \tilde{s}_{yy}} = \left(\tilde{s}_{zz}\tilde{s}_{xx} - \tilde{s}_{zx}^2\right)/2, \quad \frac{\partial H_3}{\partial \tilde{s}_{zz}} = \left(\tilde{s}_{xx}\tilde{s}_{yy} - \tilde{s}_{xy}^2\right)/2,\\
&\text{(e)} \quad \frac{\partial H_3}{\partial \tilde{s}_{yz}} = \tilde{s}_{zx}\tilde{s}_{xy} - \tilde{s}_{xx}\tilde{s}_{yz}, \quad \frac{\partial H_3}{\partial \tilde{s}_{zx}} = \tilde{s}_{xy}\tilde{s}_{yz} - \tilde{s}_{yy}\tilde{s}_{zx}, \quad \frac{\partial H_3}{\partial \tilde{s}_{xy}} = \tilde{s}_{yz}\tilde{s}_{zx} - \tilde{s}_{zz}\tilde{s}_{xy}.
\end{aligned}
\tag{A.21}
$$

Expression for $\partial \tilde{s}_{rs}/\partial \sigma_{ij}$

$$
\frac{\partial \tilde{s}_{rs}}{\partial \sigma_{ij}} = L_{rsij}. \tag{A.22}
$$

A.3. Singular cases

The derivatives $\partial \tilde{S}_p/\partial H_q$ are not defined when

$$
\tilde{S}_p^2 - 2H_1\tilde{S}_p - H_2 = 0. \tag{A.23}
$$

Solving this second order equation leads to

$$
\tilde{S}_p = H_1 \pm \sqrt{H_1^2 + H_2}. \tag{A.24}
$$

Comparing with the general solution, it is found that $\partial \tilde{S}_p/\partial H_q$ is not defined for

$$
\begin{aligned}
&\text{(a)} \quad \theta = 0, \quad \tilde{S}_2 = \tilde{S}_3,\\
&\text{(b)} \quad \theta = \pi, \quad \tilde{S}_2 = \tilde{S}_1.
\end{aligned}
\tag{A.25}
$$

For Case 1 ($\theta = 0$, $\tilde{S}_2 = \tilde{S}_3$), only $\partial \tilde{S}_1/\partial H_q$ is defined but it is possible to show that

$$
\frac{\partial \phi}{\partial H_p} = \left(\frac{\partial \phi}{\partial \tilde{S}_1} - \frac{\partial \phi}{\partial \tilde{S}_2}\right)\frac{\partial \tilde{S}_1}{\partial H_p} + 3\frac{\partial \phi}{\partial \tilde{S}_2}\delta_{p1}. \tag{A.26}
$$

For Case 2 ($\theta = \pi$, $\tilde{S}_2 = \tilde{S}_1$), only $\partial \tilde{S}_3/\partial H_q$ is defined but it is possible to show that

$$
\frac{\partial \phi}{\partial H_p} = \left(\frac{\partial \phi}{\partial \tilde{S}_3} - \frac{\partial \phi}{\partial \tilde{S}_2}\right)\frac{\partial \tilde{S}_3}{\partial H_p} + 3\frac{\partial \phi}{\partial \tilde{S}_2}\delta_{p1}. \tag{A.27}
$$

A.4. Yield function second derivatives

In order to compute the tangent stiffness matrix, which is necessary in implicit finite element solutions, second order derivatives are necessary. The general form of the second derivatives is given by

$$\frac{\partial^2\phi}{\partial\sigma_{ij}\,\partial\sigma_{ab}} = q'_1 + q'_2 + q'_3 + q'_{12} + q''_1 + q''_2 + q''_3 + q''_{12}, \tag{A.28}$$

such that second order derivatives involving cross terms of $\tilde{\mathbf{S}}'$ and $\tilde{\mathbf{S}}''$ can exist. The expressions of q_1, q_2 and q_3 (prime or double prime) are for the terms that have second partial derivatives with respect to ($\tilde{S}'_i$ and $\tilde{S}'_j$) or ($\tilde{S}''_i$ and $\tilde{S}''_j$). The additional term q'_{12} is given as

$$q'_{12} = \frac{\partial^2\phi}{\partial\tilde{S}'_p\,\partial\tilde{S}''_c}\frac{\partial\tilde{S}'_p}{\partial H'_q}\frac{\partial H'_q}{\partial\tilde{s}'_{mn}}\frac{\partial\tilde{s}'_{mn}}{\partial\sigma_{ij}}\frac{\partial\tilde{S}''_c}{\partial H''_d}\frac{\partial H''_d}{\partial\tilde{s}''_{ef}}\frac{\partial\tilde{s}''_{ef}}{\partial\sigma_{ab}}. \tag{A.29}$$

The expression q''_{12} is similar with the order of differentiation for the primes and double primes being reversed. The single derivative terms are all defined above. Only a few terms pertaining to the second derivatives of Yld2004-18p are given in the following equations.

If $i = j$

$$\frac{\partial^2\phi}{\partial\tilde{S}'_i\,\partial\tilde{S}'_j} = a(a-1)\left\{\left|\tilde{S}'_i - \tilde{S}''_1\right|^{a-2} + \left|\tilde{S}'_i - \tilde{S}''_2\right|^{a-2} + \left|S'_i - \tilde{S}''_3\right|^{a-2}\right\}, \tag{A.30}$$

otherwise,

$$\frac{\partial^2\phi}{\partial\tilde{S}'_i\,\partial\tilde{S}'_j} = 0. \tag{A.31}$$

Similarly, if $i = j$

$$\frac{\partial^2\phi}{\partial\tilde{S}''_i\,\partial\tilde{S}''_j} = a(a-1)\left\{\left|\tilde{S}'_1 - \tilde{S}''_i\right|^{a-2} + \left|\tilde{S}'_2 - \tilde{S}''_i\right|^{a-2} + \left|\tilde{S}'_3 - \tilde{S}''_i\right|^{a-2}\right\}, \tag{A.32}$$

otherwise,

$$\frac{\partial^2\phi}{\partial\tilde{S}''_i\,\partial\tilde{S}''_j} = 0. \tag{A.33}$$

For the cross terms

$$\frac{\partial^2\phi}{\partial\tilde{S}'_i\,\partial\tilde{S}''_j} = -a(a-1)\left|\tilde{S}'_i - \tilde{S}''_j\right|^{a-2}. \tag{A.34}$$

In the case of multiple roots for $\tilde{S}'_i$ or $\tilde{S}''_j$ (singular cases), there are four possible solutions for the second derivatives.

Appendix B. Error function

In order to compute and optimize the anisotropy coefficients, an error function is minimized. For in-plane tension at φ degrees from the rolling direction, the corresponding stress tensor expressed in the material frame, can be represented as the following column vector of rank 6

$$\boldsymbol{\sigma} = \left[\, \sigma_\varphi \cos^2\varphi \quad \sigma_\varphi \sin^2\varphi \quad 0 \quad 0 \quad 0 \quad \sigma_\varphi \sin\varphi\cos\varphi \,\right]^{\mathrm{T}}, \tag{B.1}$$

where σ_φ is the flow stress in the corresponding direction. Thus, the stress deviator is

$$\mathbf{s} = \sigma_\varphi \left[\left(\cos^2\varphi - 1/3\right) \quad \left(\sin^2\varphi - 1/3\right) \quad -1/3 \quad 0 \quad 0 \quad \sin\varphi\cos\varphi \right]^{\mathrm{T}} = \sigma_\varphi \mathbf{s}_\varphi. \tag{B.2}$$

The flow stress σ_φ is given by

$$\frac{\sigma_\varphi}{\bar{\sigma}} = \left(\frac{K}{\phi\left(\mathbf{s}_\varphi\right)} \right)^{1/a}, \tag{B.3}$$

where K is equal to 4 for Yld2004-18p and 2 for Yld2004-13p. The r value is given by

$$r_\varphi = -1 - \frac{Ka}{\left.\frac{\sigma_\varphi}{\bar{\sigma}} \frac{\partial\phi}{\partial s_{zz}}\right|_{\mathbf{s}_\varphi}}. \tag{B.4}$$

For in-plane balanced biaxial tension, the stress state is represented by

$$\mathbf{s} = \sigma_{\mathrm{b}} [\, -1/3 \quad -1/3 \quad 2/3 \quad 0 \quad 0 \quad 0 \,]^{\mathrm{T}} = \sigma_{\mathrm{b}} \mathbf{s}_{\mathrm{b}}. \tag{B.5}$$

The flow stress σ_{b} and biaxial r value r_{b} are respectively

$$\frac{\sigma_{\mathrm{b}}}{\bar{\sigma}} = \left(\frac{K}{\phi(\mathbf{s}_{\mathrm{b}})} \right)^{1/a}, \tag{B.6}$$

$$r_{\mathrm{b}} = \frac{\partial\phi/\partial s_{yy}}{\partial\phi/\partial s_{xx}}. \tag{B.7}$$

The out-of-plane flow stresses are

$$\frac{\sigma_q}{\bar{\sigma}} = \left(\frac{K}{\phi\left(\mathbf{s}_q\right)} \right)^{1/a}, \tag{B.8}$$

where $\mathbf{s}_q$ is

$$\mathbf{s}_q = \sigma_q [\, -1/3 \quad 1/6 \quad 1/6 \quad 1/2 \quad 0 \quad 0 \,]^{\mathrm{T}} \quad \text{for } 45^\circ \text{ tension in (TD–ND) plane,} \tag{B.9}$$

$$\mathbf{s}_q = \sigma_q [\, 1/6 \quad -1/3 \quad 1/6 \quad 0 \quad 1/2 \quad 0 \,]^{\mathrm{T}} \quad \text{for } 45^\circ \text{ tension in (ND, RD) plane,} \tag{B.10}$$

$$\mathbf{s}_q = \sigma_q[0 \quad 0 \quad 0 \quad 1 \quad 0 \quad 0]^{\mathrm{T}} \quad \text{for simple shear in (TD–ND) plane,} \tag{B.11}$$

$$\mathbf{s}_q = \sigma_q[0 \quad 0 \quad 0 \quad 0 \quad 1 \quad 0]^{\mathrm{T}} \quad \text{for simple shear in (ND, RD) plane.} \tag{B.12}$$

The error function is defined by

$$E\left(c'_{ij}, c''_{ij}\right) = \sum_p w_p \left(\frac{\sigma_p^{\mathrm{pr}}}{\sigma_p^{\mathrm{ex}}} - 1\right)^2 + \sum_q w_q \left(\frac{r_q^{\mathrm{pr}}}{r_q^{\mathrm{ex}}} - 1\right)^2, \tag{B.13}$$

where p represents the number of experimental flow stresses available, either in uniaxial tension or simple shear in different directions, and q represents the number of experimental r values. In the above equation, the superscript denotes whether the corresponding value is experimental or predicted. Each term in the error function is weighted by w. The weight can be used to differentiate flow stresses or r values. For the flow stress, a better accuracy is required because a difference of a few percent is significant while it is not in r value. Moreover, experimental and predicted flow stress variation range is smaller than that of the r values. Finally, because some of the input data are not known but approximated by the isotropic value or computed with a polycrystal model (pseudo-experimental values), the weight corresponding to these input data is made lower than the weight of the experimental data, which are more reliable. Typically, in this work, weights for the in-plane flow stresses and r values in uniaxial tension, and the other flow stresses were 1.00, 0.10 and 0.01, respectively.

Appendix C. Numerical differentiation

The yield function gradient emerging in the associated flow rule (A.17) may alternatively and very conveniently be calculated by means of numerical differentiation methods. In Aretz (2003) a central, as well as a forward difference scheme, has been presented for this purpose. It was shown that for 3D stress states the computational effort for the central difference scheme is approximately 1.7 times larger compared to the forward difference scheme while no practical differences concerning accuracy have been observed. Thus, the forward difference scheme will be presented here as an interesting alternative to the analytical computation of the yield function gradient. It has also been pointed out in Aretz (2003) that the singularities in the gradient expressions are easily avoided and that the implementation of anisotropic yield functions can be simplified significantly if numerical differentiation is employed.

The forward difference expressions for the yield function gradient components are as follows:

$$\frac{\partial \phi}{\partial \boldsymbol{\sigma}} \approx \frac{\phi(\boldsymbol{\sigma} + \Delta\boldsymbol{\sigma}) - \phi(\boldsymbol{\sigma})}{\Delta\boldsymbol{\sigma}}, \tag{C.1}$$

where the module of $\Delta\boldsymbol{\sigma}$ is $\|\Delta\boldsymbol{\sigma}\| = \Delta\sigma$. In (Aretz, 2003) $\Delta\sigma \approx 10^{-5}$ has been found to be a reasonable choice for typical metal forming applications.

Appendix D. Calculation of r_b from YLD96

If r_b cannot be obtained from the disk compression test or from a crystal plasticity calculation, it can be calculated from another yield function (Barlat et al., 1997), denoted Yld96. The procedure consists in solving for the five coefficients of the Yld96 yield locus (no shear stress) and to calculate r_b, assuming the associated flow rule. The required non-linear system of five equations of the five unknown α_x, α_y, c_1, c_2, c_3 is

$$
\begin{aligned}
&\text{(a)}\quad \alpha_x|c_2-c_3|^a+\alpha_y|2c_2+c_3|^a+|c_2+2c_3|^a=2(3\bar{\sigma}/\sigma_0)^a,\\
&\text{(b)}\quad \alpha_x|c_3+2c_1|^a+\alpha_y|c_3-c_1|^a+|2c_3+c_1|^a=2(3\bar{\sigma}/\sigma_{90})^a,\\
&\text{(c)}\quad \alpha_x|2c_1+c_2|^a+\alpha_y|c_1+2c_2|^a+|c_1-c_2|^a=2(3\bar{\sigma}/\sigma_b)^a,\\
&\text{(d)}\quad -\alpha_x[r_0(2c_1+c_2)+(c_3+2c_1)](c_2-c_3)|c_2-c_3|^{a-2}\\
&\qquad -\alpha_y[r_0(c_1+2c_2)-(c_3-c_1)](2c_2+c_3)|2c_2+c_3|^{a-2}\\
&\qquad +[r_0(c_1-c_2)+(2c_3+c_1)](c_2+2c_3)|c_2+2c_3|^{a-2}=0,\\
&\text{(e)}\quad \alpha_x[(c_2-c_3)/r_{90}+(2c_1+c_2)](c_3+2c_1)|c_3+2c_1|^{a-2}\\
&\qquad -\alpha_y[(2c_2+c_3)/r_{90}+(c_1+2c_2)](c_3-c_1)|c_3-c_1|^{a-2}\\
&\qquad -[(c_2+2c_3)/r_{90}-(c_1-c_2)](2c_3+c_1)|2c_3+c_1|^{a-2}=0.
\end{aligned}
\tag{D.1}
$$

After solving this system numerically, for instance with a Newton-Raphson solver, r_b is given by

$$
\begin{aligned}
r_b=&\Big[-\alpha_x(c_3+2c_1)(2c_1+c_2)|2c_1+c_2|^{a-2}+\alpha_y(c_3-c_1)(c_1+2c_2)|c_1+2c_2|^{a-2}\\
&-(2c_3+c_1)(c_1-c_2)|c_1-c_2|^{a-2}\Big]\Big/\Big[-\alpha_x(c_2-c_3)(2c_1+c_2)|2c_1+c_2|^{a-2}\\
&-\alpha_y(2c_2+c_3)(c_1+2c_2)|c_1+2c_2|^{a-2}+(c_2+2c_3)(c_1-c_2)|c_1-c_2|^{a-2}\Big].
\end{aligned}
\tag{D.2}
$$

References

Aretz, H., 2003. Modellierung des anisotropen Materialverhaltens von Blechen mit Hilfe der Finite-Elemente-Methode. Doctoral thesis, RWTH Aachen University, Shaker-Verlag (2003), Germany.

Banabic, D., 2001. Anisotropy of sheet Metals. In: Banabic, D. (Ed.), Formability of Metallic Materials. Springer, Berlin, pp. 119–172.

Banabic, D., Cazacu, O., Barlat, F., Comsa, D.S., Wagner, S., Siegert, K., 2003. Description of anisotropic behaviour of AA3103-0 aluminium alloy using two recent yield criteria. J. Phys. IV 105, 297–304.

Banabic, D., Aretz, H., Comsa, D.S., Paraianu, L, 2004. An improved analytical description of orthotropy in metallic sheets. Int. J. Plasticity, in press.

Barlat, F., Lian, J., 1989. Plastic behavior and stretchability of sheet metals. Part I: A yield function for orthotropic sheets under plane stress conditions. Int. J. Plasticity 5, 51–56.

Barlat, F., Liu, J., 1998. Modeling precipitate-induced anisotropy in binary Al–Cu alloys. Mater. Sci. Eng. A257, 47–61.

Barlat, F., Lege, D.J., Brem, J.C., 1991. A six-component yield function for anisotropic materials. Int. J. Plasticity 7, 693–712.

Barlat, F., Maeda, Y., Chung, K., Yanagawa, M., Brem, J.C., Hayashida, Y., Lege, D.J., Matsui, K., Murtha, S.J., Hattori, S., Becker, R.C., Makosey, S., 1997. Yield function development for aluminum alloy sheets. J. Mech. Phys. Solids 45, 1727–1763.

Barlat, F., Banabic, D., Cazacu, O., 2002. Anisotropy in sheet metals. In: Yang, D.Y., Oh, S.I., Huh, H., Kim, Y.H., (Eds.), Proceedings of the Fifth International Conference and Workshop on Numerical Simulation of 3D Sheet Forming Processes, Jeju Island, Korea, October 2002, pp. 515–524.

Barlat, F., Brem, J.C., Yoon, J.W., Chung, K., Dick, R.E., Lege, D.J., Pourboghrat, F., Choi, S.-H., Chu, E., 2003. Plane stress yield function for aluminum alloy sheet. Part I: Theory. Int. J. Plasticity 19, 1297–1319.

Barlat, F., Cazacu, O., Życzkowski, M., Banabic, D., Yoon, J.W., 2004. Yield surface plasticity and anisotropy. In: Raabe, D., Chen, L.-Q., Barlat, F., Roters, F. (Eds.), Continuum Scale Simulation of Engineering Materials Fundamentals – Microstructures – Process Applications. WILEY–VCH Verlag, Berlin GmbH, pp. 145–177.

Bishop, J.F.W., Hill, R., 1951. A theory of the plastic distortion of a polycrystalline aggregate under combined stresses. Phil. Mag. 42, 414–427.

Boehler, J.P., Sawczuk, A., 1970. Equilibre limite des sols anisotropes. J. Mécanique 9, 5–33.

Bourne, L., Hill, R., 1950. On the correlation of the directional properties of rolled sheet in tension and cupping tests. Phil. Mag. 41, 671–681.

Bron, F., Besson, J., 2004. A yield function for anisotropic materials. Application to aluminum alloys. Int. J. Plasticity 20, 937–963.

Cazacu, O., Barlat, F., 2001. Generalization of Drucker's yield criterion to orthotropy. Math. Mech. Solids 6, 613–630.

Cazacu, O., Barlat, F., 2003. Application of the theory of representation to describe yielding of anisotropic aluminum alloys. Int. J. Eng. Sci. 41, 1367–1385.

Cazacu, O., Barlat, F., 2004. A criterion for description of anisotropy and yield differential effects in pressure-insensitive materials. Int. J. Plasticity 20, 2027–2045.

Hecker, S.S., 1976. Experimental studies of yield phenomena in biaxially loaded metals. In: Stricklin, A., Saczalski, K.C. (Eds.), Constitutive Modeling in Viscoplasticity. ASME, New-York, pp. 1–33.

Hershey, A.V., 1954. The plasticity of an isotropic aggregate of anisotropic face centred cubic crystals. J. Appl. Mech. 21, 241–249.

Hill, R., 1948. A theory of the yielding and plastic flow of anisotropic metals. Proc. Roy. Soc. London A193, 281–297.

Hosford, W.F., 1972. A generalized isotropic yield criterion. J. Appl. Mech. Trans. ASME 39, 607–609.

Karafillis, A.P., Boyce, M.C., 1993. A general anisotropic yield criterion using bounds and a transformation weighting tensor. J. Mech. Phys. Solids 41, 1859–1886.

Lebensohn, R., Tomé, C.N., 1993. A self-consistent anisotropic approach for the simulation of plastic deformation and texture development of polycrystals: Application to zirconium alloys. Acta Metall. Mater. 41, 2611–2624.

Lippman, H., 1970. Matrixungleichungen und die Konvexität der Fliessfläche. Zeit. Angew. Mech. 50, 134–137.

Liu, S.I., 1982. On representations of anisotropic invariants. Int. J. Eng. Sci. 20, 1099–1109.

Logan, R.W., Hosford, W.F., 1980. Upper-bound anisotropic yield locus calculations assuming pencil glide. Int. J. Mech. Sci. 22, 419–430.

Paul, B., 1968. Macroscopic criteria for plastic flow and brittle fracture. In: Liebowitz, H. (Ed.), Fracture, vol. 1. Academic Press, San Diego, CA, pp. 313–495.

Peeters, B., Seefeldt, M., Teodosiu, C., Kalindindi, S.R., Van Houtte, P., Aernould, E., 2001. Work hardening/softening behaviour of b.c.c. polycrystals during changing strain path: II. An integrated model based on substructure and texture evolution, and its predictions of the stress–strain behaviour of an IF steel during two-stage strain paths. Acta Mater. 49, 1607–1619.

Richmond, O., Spitzig, W.A., 1980. Pressure dependence and dilatancy of plastic flow. , IUTAM Conference, Theoretical and Applied Mechanics, Proceedings of the 15th International Congress of Theoretical and Applied Mechanics. North-Holland Publishers, Amsterdam, pp. 377–386.

Rockafellar, R.T., 1972. Convex Analysis. Princeton University Press, Princeton, NY.

Sobotka, Z., 1969. Theorie des plastischen Fliessens von anisotropen Körpern. Zeit. Angew. Math. Mech. 49, 25–32.

Spitzig, W.A., Richmond, O., 1984. The effect of pressure on the flow stress of metals. Acta Metall. 32, 457–463.

Spitzig, W.A, Sober, R.J., Richmond, O., 1976. The effect of hydrostatic pressure on the deformation behavior of Maraging and HY-80 steels and its implication for plasticity theory. Metall. Trans. 7A, 1703–1710.

Teodosiu, C., Hu, Z., 1998. Microstructure in the continuum modeling of plastic anisotropy. In: Cartensen, J.V., Leffers, T., Lorentzen, T., Pedersen, O.B., Sørensen, B.F., Winther, G. (Eds.), Proceedings of the Risø International Symposium on Material Science: Modelling of Structure and Mechanics of Materials from Microscale to products. Risø National Laboratory, Roskilde, Denmark, pp. 149–168.

Tong, W., 2004. A planar anisotropic plastic flow theory for monoclinic sheet metals. Int. J. Mech. Sci., submitted for publication.

Von Mises, R., 1928. Mechanics der plastischen Formänderung von Kristallen. Zeitschrift Angewandte Mathematik Mechanik 8, 161–185.

Wang, C.C., 1970. A new representation theorem for isotropic functions, Part I and II. Arch. Rat. Mech. An. 36, 166–223.

Young, R.F., Bird, J.E., Duncan, J.L., 1981. An automated hydraulic bulge tester. J. Appl. Metalwork 2, 11–18.

Yu, M.H., 2002. Advances in strength theories for materials under complex stress state in the 20th Century. Appl. Mech. Rev. 55, 198–218.

Życzkowski, M., 1981. Combined Loadings in the Theory of Plasticity. Polish Scientific Publisher, Warsaw.

Życzkowski, M., 2001. Anisotropic yield conditions. In: Lemaitre, J. (Ed.), Handbook of Materials Behavior Models. Academic Press, San Diego, CA, pp. 155–165.